Quantum entangled ground states of two spinor Bose-Einstein condensates

Z. F. Xu,* R. Lü, and L. You

State Key Laboratory of Low Dimensional Quantum Physics, Department of Physics, Tsinghua University, Beijing 100084, China

(Received 26 October 2011; published 27 December 2011)

We revisit in detail the non-mean-field ground-state phase diagram for a binary mixture of spin-1 Bose-Einstein condensates including quantum fluctuations. The noncommuting terms in the spin-dependent Hamiltonian under the single-spatial-mode approximation make it difficult to obtain exact eigenstates. Utilizing spin-z-component conservation and total spin angular momentum conservation, we numerically derive information on the building blocks and evaluate the von Neumann entropy to quantify the ground states. The mean-field phase boundaries are found to remain largely intact, yet the ground states show fragmented and entangled behaviors within large parameter spaces of interspecies spin-exchange and singlet-pairing interactions.

DOI: 10.1103/PhysRevA.84.063634 PACS number(s): 03.75.Mn, 03.75.Gg

I. INTRODUCTION

Ultracold atomic quantum gases with spin degrees of freedom provide exceptionally clean and idealized testing beds for studying quantum magnetism [1,2]. Optical trapping from ac Stark shifts of off-resonant laser fields is capable of equal confinement for all atomic pseudospin components, which facilitates research into exciting spinor physics with atomic quantum gases. As is often done in studying a trapped Bose gas, when treating the condensate, we first take a mean-field (MF) approximation assuming that only one eigenvalue of the single-particle density matrix is macroscopic, being of order N. Second quantization is then limited to the condensate mode. Such a simple scenario already allows for many interesting quantum many-body phenomena [3].

Two popular atomic species often employed in experimental research on spinor Bose-Einstein condensates (BECs) [3–9] are ^{87}Rb and ^{23}Na atoms. Within each species, their interactions are dominated by the density-dependent interaction in comparison to the much weaker spin-dependent interactions. As a result, a single-spatial mode approximation (SMA), whereby the spatial dependence of the condensate wave function is determined independently of the spin degrees of freedom, was introduced [6] and remains reasonable as long as the number of atoms is not too large [10]. Within the MF approximation, the ground state of a spinor BEC is found to be ferromagnetic, polar, or cyclic phases, etc., determined by the spin-dependent interactions and the total (hyperfine) spin F of the atom. Further theoretical work armed with full quantum calculations revealed interesting many-body states [6,7,9,11], beyond the scope of those from MF approximations. For spin-1 condensates, the exact eigenstates will contain paired spin singlets [6,7,11], which become more complex for higher spin condensates. For example, the spin-2 case involves spin singlets which can be formed by either two or three atoms [7,9]. A general procedure exists for more detailed information on the building blocks of eigenstates determined by their associated generating functions [12]. More generally, we can always resort to the means of numerics to diagonalize the ground-state single-particle density matrix, which then reveals fragmented ground states if more than one eigenvalue is of order N [13].

Several groups have recently studied spinor condensate mixtures [17–24], which also display non-MF features, such as anomalous quantum fluctuations for each spin component and quantum entangled ground states. This was first discovered in spinor condensates with more than one orbital, for instance, the case of pseudo-spin-1/2 condensates [14–16], for which Kuklov and Svistunov [14] predicted that in the ground states all atoms will have to condense into two orthogonal spatial orbitals or more due to the conservation of the total spin. This could result in a condensate ground state being a maximally entangled many-body state. Shi *et al.* replaced the two orbitals with two different atomic species; a ground state with entangled order parameter followed [16]. Under MF approximation, we have previously elaborated the ground-state phase diagram for a condensate mixture of two spin-1 BECs [18]. The interesting phases are named, appropriately, the FF, AA, PP, CC, and MM phases, distinguishing different structures and interaction parameter spaces. Furthermore, we provide many beyond-MF results based on a full quantum spin-dependent Hamiltonian [19], which contains noncommuting terms, forbidding a simple derivation of the exact eigenstates. For two special cases, commutations are restored among the generally noncommuting terms. First, when the interspecies singlet pairing interaction is ignored ($\gamma = 0$), the Hamiltonian is then simply composed of three operators which obey the angular momentum algebra. Making use of the eigenstates of single spin-1 condensates, we directly construct the eigenstates of a binary spin-1 mixture using the angular momentum coupling representation. Second, when the interspecies antiferromagnetic spin-exchange interaction is strong enough, the ground state will be forced to develop entanglement between the two species [19], a result consistent with what is discovered in a spin-1 condensate placed inside a double well [25]. Other interesting features are discussed for $\gamma = 0$, revealing fragmentation and quantum entanglement [20,21,23].

II. THE MODEL HAMILTONIAN

In this revisit we hope to understand quantum entanglement between two spin-1 condensates when both interspecies spin-exchange and singlet-pairing interactions are present.

*zfxu83@gmail.com

Our study is based on the same model system of a binary mixture of spin-1 condensates confined in optical traps. The corresponding field operators that annihilates a boson of species 1 and species 2 at position $\mathbf{r}$ are described, respectively, by $\hat{\Psi}_{M_F}(\mathbf{r})$ and $\hat{\Phi}_{M_F}(\mathbf{r})$, where $M_F = -1,0,1$, denoting the three Zeeman hyperfine states. The SMA is adopted for each of the two species, employing two spatial mode functions, $\psi(\mathbf{r})$ and $\phi(\mathbf{r})$, respectively, and the field operators are expanded as $\hat{\Psi}_{M_F}(\mathbf{r}) = \hat{a}_{M_F}\psi(\mathbf{r})$ and $\hat{\Phi}_{M_F}(\mathbf{r}) = \hat{b}_{M_F}\phi(\mathbf{r})$, with $\hat{a}_{M_F}$ and $\hat{b}_{M_F}$, respectively, the annihilation operators for an atom in the spin component M_F. In the absence of an external magnetic field, the spin-dependent Hamiltonian for a binary mixture of spin-1 condensates then becomes

$$\begin{aligned}\hat{H}_s = {} & \tfrac{1}{2}C_1\beta_1\big(\hat{L}_1^2 - 2\hat{N}_1\big) + \tfrac{1}{2}C_2\beta_2\big(\hat{L}_2^2 - 2\hat{N}_2\big) \\ & + \tfrac{1}{2}C_{12}\beta\hat{\mathbf{L}}_1\cdot\hat{\mathbf{L}}_2 + \tfrac{1}{6}C_{12}\gamma\hat{\Theta}_{12}^\dagger\hat{\Theta}_{12} \end{aligned} \tag{1}$$

under the SMA [19]. The interaction coefficients are $C_1 = \int d\mathbf{r}|\psi(\mathbf{r})|^4$, $C_2 = \int d\mathbf{r}|\phi(\mathbf{r})|^4$, and $C_{12} = \int d\mathbf{r}|\psi(\mathbf{r})|^2|\phi(\mathbf{r})|^2$. β_1 (β_2) is the intraspecies spin-exchange interaction parameter of species 1 (2). β and γ denote inter-species spin-exchange and singlet-pairing interaction parameters, respectively. The singlet pairing operator becomes $\hat{\Theta}_{12}^\dagger = \hat{a}_1^\dagger\hat{b}_{-1}^\dagger - \hat{a}_0^\dagger\hat{b}_0^\dagger + \hat{a}_{-1}^\dagger\hat{b}_1^\dagger$, and two angular-momentum-like operators, $\hat{\mathbf{L}}_1 = \sum_{ij}\hat{a}_i^\dagger\mathbf{F}_{ij}\hat{a}_j$ and $\hat{\mathbf{L}}_2 = \sum_{ij}\hat{b}_i^\dagger\mathbf{F}_{ij}\hat{b}_j$, obey the usual angular momentum algebra [6,26]. They commute with atom number operators $\hat{N}_1 = \sum_i\hat{a}_i^\dagger\hat{a}_i$ and $\hat{N}_2 = \sum_i\hat{b}_i^\dagger\hat{b}_i$. In the above, $\mathbf{F}_{ij}$ denotes the (i,j) component of the spin-1 matrix $\mathbf{F}$.

III. GROUND-STATE PHASE DIAGRAM

As presented in Ref. [19], for the spin-dependent Hamiltonian, Eq. (1), the first three terms commute with each other, but they do not commute with the fourth term. This shows that the ground state determined will depend on the interaction parameters. As a result, we resorted to the special cases of no interspecies singlet-pairing interaction ($\gamma = 0$) and $C_1\beta_1 = C_2\beta_2 = C_{12}\beta/2$ [19]. The first case, $\gamma = 0$, has already attracted much attention due to the appearance of fragmented ground states and the associated entanglement between two species and exotic atomic number fluctuations [19–21].

In this study, we discuss the general case of the full spin-dependent Hamiltonian, Eq. (1). Whenever the ground state depends on the interaction parameters, we have to perform a full quantum calculation numerically; usually this amounts to a full exact numerical diagonalization for both atom numbers, N_1 and N_2. Before discussing the numerical results, we want to point out that there still exist two conserved quantities—the total spin angular momentum and its z component—as $\hat{L}^2 = (\hat{L}_1 + \hat{L}_2)^2$ commutes with the spin-dependent Hamiltonian. As a result, we can elaborate spin structures from building blocks derived by generating the function of the maximum spin states $|l,l_z = l\rangle$, where we have used quantum numbers l and l_z to denote the common eigenstates of the angular momentum operators $\hat{L}^2$ and $\hat{L}_z$.

We recall the suitable generating function $G_g(x,y,z)$ for a binary mixture of two spin-1 condensates derived in Ref. [19]. From this generating function, we have figured out all six building blocks for constructing the eigenstate $|l,l\rangle$, which is given by

$$\begin{aligned}|l,l\rangle = {} & \sum\mathcal{C}(\{u_i\},\{v_i\},\{w_i\})\big(\hat{A}_1^{(1)\dagger}\big)^{u_1}\big(\hat{A}_0^{(2)\dagger}\big)^{u_2}\big(\hat{B}_1^{(1)\dagger}\big)^{v_1} \\ & \times\big(\hat{B}_0^{(2)\dagger}\big)^{v_2}\big(\hat{\Gamma}_0^{(1,1)\dagger}\big)^{w_1}\big(\hat{\Gamma}_1^{(1,1)\dagger}\big)^{w_2}|\mathrm{vac}\rangle, \end{aligned} \tag{2}$$

where the six building blocks are

$$\begin{aligned}\hat{A}_1^{(1)\dagger} &= \hat{a}_1^\dagger, \quad \hat{A}_0^{(2)\dagger} = \hat{a}_0^{\dagger 2} - 2\hat{a}_1^\dagger\hat{a}_{-1}^\dagger, \\ \hat{B}_1^{(1)\dagger} &= \hat{b}_1^\dagger, \quad \hat{B}_0^{(2)\dagger} = \hat{b}_0^{\dagger 2} - 2\hat{b}_1^\dagger\hat{b}_{-1}^\dagger, \\ \hat{\Gamma}_0^{(1,1)\dagger} &= \hat{\Theta}_{12}^\dagger, \quad \hat{\Gamma}_1^{(1,1)\dagger} = \frac{1}{\sqrt{2}}(\hat{a}_1^\dagger\hat{b}_0^\dagger - \hat{a}_0^\dagger\hat{b}_1^\dagger), \end{aligned} \tag{3}$$

and u_i, v_i, and w_i satisfy the constraints

$$\begin{aligned} u_1 + 2u_2 + w_1 + w_2 &= N_1, \\ v_1 + 2v_2 + w_1 + w_2 &= N_2, \\ u_1 + v_1 + w_2 &= l, \end{aligned} \tag{4}$$

and additionally, $w_2 = 0,1$. Spin states $|l,l_z \neq l\rangle$ of other magnetizations can be constructed by simply applying $\hat{L}_-^{l-l_z}$ on state $|l,l\rangle$ as $\hat{L}_-^{l-l_z}|l,l\rangle \propto |l,l_z \neq l\rangle$ (non-normalized).

In most numerical studies, we assume that each species contains 100 atoms ($N_1 = N_2 = N = 100$). Due to the SO(3) symmetry of our model, we restrict the Hilbert space to the subspace of zero magnetization with $l_z = 0$ [27]. In Fig. 1, we summarize the extensive numerical results. Since the total spin angular momentum is conserved, we can use the eigenvalue of the operator $\hat{L}^2$ to distinguish different phase; this is then accompanied by the information on the building blocks. A total of three constraints exists for the allowed values of u_i, v_i, and w_i ($i = 1,2$). Only three are needed for a solution; we choose the three as u_2, v_2, and w_1, which are determined numerically by evaluating the associated expectation values of $\hat{A}_0^{(2)\dagger}\hat{A}_0^{(2)}$, $\hat{B}_0^{(2)\dagger}\hat{B}_0^{(2)}$, and $\hat{\Gamma}_0^{(1,1)\dagger}\hat{\Gamma}_0^{(1,1)}$, respectively.

From the extensive numerical results we construct the ground-state phase diagram as shown in Fig. 1. Perhaps not surprisingly, it is almost the same as the MF approximation studied in Ref. [18]. Each phase is then labeled the same as before [18], albeit that the meanings can be different due to the noncommuting operators in the spin-dependent Hamiltonian, Eq. (1). In Table I, we summarize the properties for the four special phases: FF, AA, PP, and CC. The remaining MM phase still denotes the phase whose parameters evolve continuously across the phase boundaries.

IV. ENTANGLED GROUND STATES

To quantify entanglement between the two species, we numerically computed the von Neumann entropy $S(\hat{\rho}_1) = -\mathrm{Tr}(\hat{\rho}_1\log_{2N+1}\hat{\rho}_1)$, where $\hat{\rho}_1 = \mathrm{Tr}_2\hat{\rho}$ is the reduced density matrix resulting from partial tracing of the ground-state density matrix $\hat{\rho}$ over the basis of species 2. The amount of entanglement is then shown as density plots over the phase diagram in Fig. 1, with the legend shown at the right; the black (white) color refers to low (high) entanglement.

In the absence of interspecies singlet-pairing interaction ($\gamma = 0$), the spin-dependent Hamiltonian, Eq. (1), contains only three operators commuting with each other. As a result,

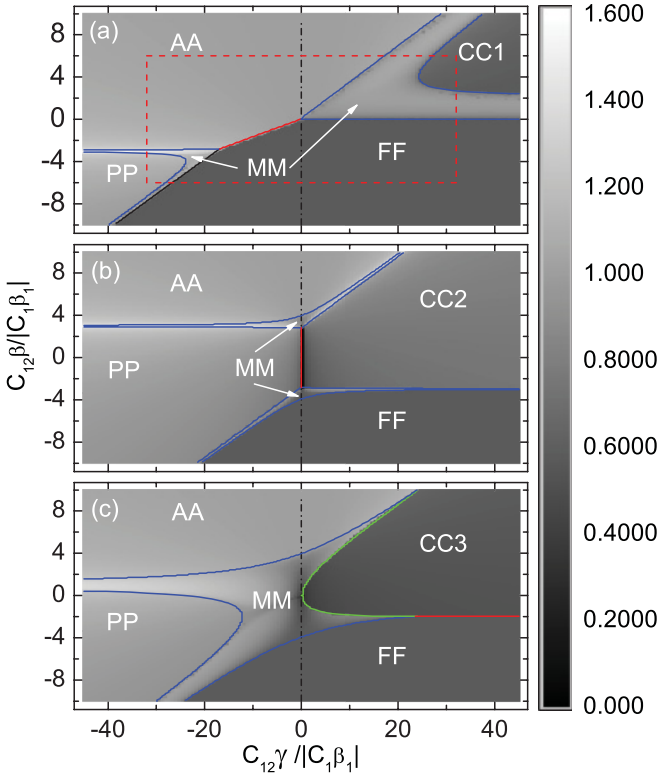

FIG. 1. (Color online) Ground-state phase diagram and corresponding von Neumann entropy distribution at fixed values of $C_1\beta_1$ and $C_2\beta_2$. Solid blue lines denote continuous phase transition boundaries between the MM phase and the FF, PP, AA, CC1, and CC2 phases. Solid red lines denote discontinuous phase transition between phases (AA and FF, PP and CC2, FF and CC3) with fully determined total spin angular momentum l. The solid green line denotes the discontinuous phase transition boundary between the CC3 phase and the MM phase. Vertical dash-dotted lines correspond to $C_{12}\gamma = 0$ and serve as guides for the eye. The von Neumann entropies of the ground states are illustrated as grayscale density plots, where black (white) refers to low (high) entanglement, respectively. The three subplots denote fixed intraspecies spin exchange interaction parameters of $(C_1\beta_1, C_2\beta_2)/|C_1\beta_1|$ equal to (a) $(-1,-2)$, (b) $(1,2)$, and (c) $(-1,2)$. Dashed (red) rectangle in (a) shows four lines connecting the points $O_{\rm AA}(-32,6)$, $O_{\rm CC}(32,6)$, $O_{\rm FF}(32,-6)$, and $O_{\rm PP}(-32,-6)$ in the parameter space of $(C_{12}\gamma, C_{12}\beta)/|C_1\beta_1|$.

we can use quantum numbers l_1, l_2, l, and l_z to quantify its eigenstate $|l_1,l_2,l,l_z\rangle$, with $\langle \hat{L}_1^2\rangle = l_1(l_1+1)$, $\langle \hat{L}_2^2\rangle = l_2(l_2+1)$, $\langle \hat{L}^2\rangle = l(l+1)$, and $\langle \hat{L}_z\rangle = l_z$. In the ground states, we have $l = l_1 + l_2$ for ferromagnetic interspecies spin-exchange interaction ($\beta < 0$) and $l = |l_1 - l_2|$ for antiferromagnetic interspecies spin-exchange interaction ($\beta > 0$), while the values of l_1 and l_2 are determined by the three interaction parameters.

In Fig. 2, we display the expected values of the intra- and interspecies single-pairing number operators in the ground state, divided by their corresponding maximum values shown in Table I. In addition, we show the total spin angular momentum and the von Neumann entropy. First, when $\beta_1 < 0$, $\beta_2 < 0$, irrespective of the interspecies spin-exchange interaction, atoms in the same species will not pair into a singlet, but atoms in different species will pair into singlets, with $\langle \Gamma_0^{(1,1)\dagger}\Gamma_0^{(1,1)}\rangle$

TABLE I. Expectation values for the special operators in the ground state within different phases.

	$\langle \hat{L}^2\rangle$	$\langle \hat{A}_0^{(2)\dagger}\hat{A}_0^{(2)}\rangle$	$\langle \hat{B}_0^{(2)\dagger}\hat{B}_0^{(2)}\rangle$	$\langle \hat{\Gamma}_0^{(1,1)\dagger}\hat{\Gamma}_0^{(1,1)}\rangle$
FF	$2N(2N+1)$	0	0	0
AA	0	~ 0	~ 0	$\sim N(N+2)$
PP	0	$\sim N(N+1)$	$\sim N(N+1)$	~ 0
CC1	$N(N+1)$	$\sim N(N+1)$	~ 0	$\sim N(N+2)$
CC2	0	$\sim N(N+1)$	$\sim N(N+1)$	$\sim N(N+2)$
CC3	$N(N+1)$	~ 0	$\sim N(N+1)$	$\sim N(N+2)$

close to reaching its maximum values $N(N+2)$ when the interspecies spin-exchange interaction is antiferromagnetic. The corresponding total spin angular momentum $\hat{L}^2$ is equal to its maximum value $2N(2N+1)$ with a relatively low von Neumann entropy when the interspecies spin-exchange interaction is ferromagnetic. The total spin angular momentum $\hat{L}^2$ is equal to 0 with the von Neumann entropy $S(\hat{\rho}_1) = 1$ for antiferromagnetic interspecies spin-exchange interaction. Second, when $\beta_1 > 0$, $\beta_2 > 0$, in the two limits of large ferromagnetic or antiferromagnetic interspecies spin-exchange interaction, the ground state is the same as above in the previous case. In the other limit, with low interspecies spin-exchange interaction, atoms in the same species tend to pair into singlets, giving rise to no entanglement between the two species. This implies that the ground state can be written

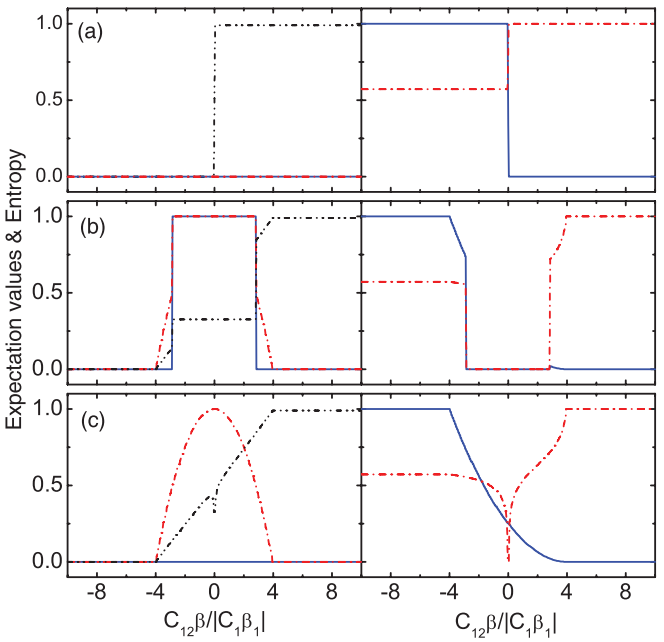

FIG. 2. (Color online) Left: Ground-state normalized expectation values of intra- and interspecies singlet-pairing number operators $\hat{A}_0^{(2)\dagger}\hat{A}_0^{(2)}/N(N+1)$, $\hat{B}_0^{(2)\dagger}\hat{B}_0^{(2)}/N(N+1)$, and $\hat{\Gamma}_0^{(1,1)\dagger}\hat{\Gamma}_0^{(1,1)}/N(N+2)$, denoted by solid (blue), dash-dotted (red), and dash-dot-dotted (black) lines, respectively. Right: Normalized total spin angular momentum $\hat{L}^2/2N(2N+1)$ and von Neumann entropy of the ground state, denoted by solid (blue) and dash-dotted (red) lines, respectively. The three subplots denote zero interspecies singlet-pairing interaction ($\gamma = 0$) and fixed intraspecies spin-exchange interaction parameters $(C_1\beta_1, C_2\beta_2)/|C_1\beta_1|$ equal to (a) $(-1,-2)$, (b) $(1,2)$, and (c) $(-1,2)$.

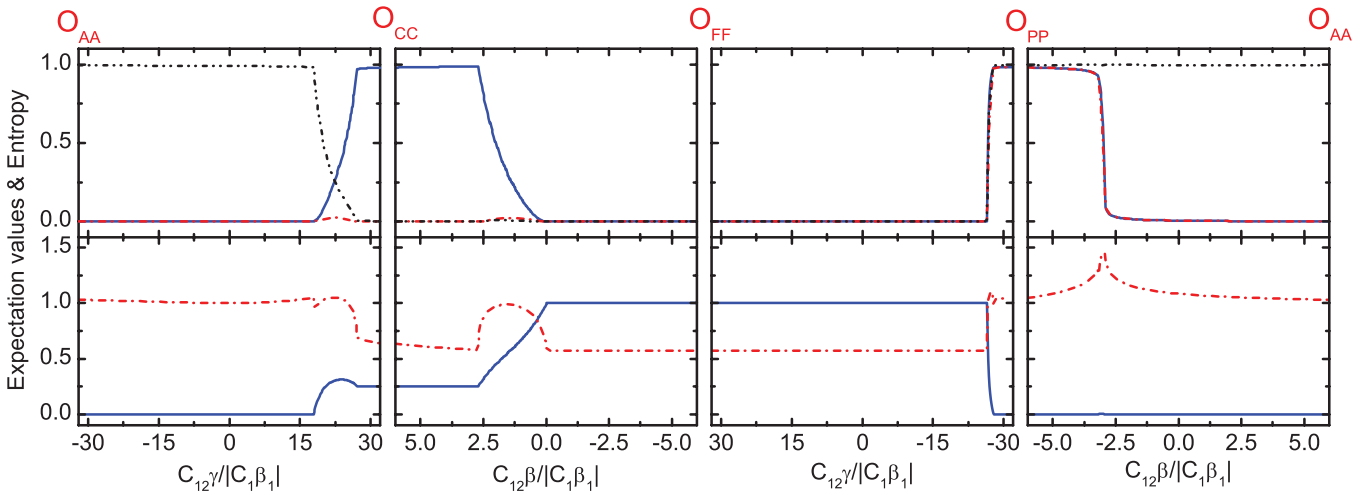

FIG. 3. (Color online) Top: Ground-state normalized expectation values of intra- and interspecies singlet-pairing number operators $\hat{A}_0^{(2)\dagger}\hat{A}_0^{(2)}/N(N+1)$, $\hat{B}_0^{(2)\dagger}\hat{B}_0^{(2)}/N(N+1)$, and $\hat{\Gamma}_0^{(1,1)\dagger}\hat{\Gamma}_0^{(1,1)}/N(N+2)$, denoted by solid (blue), dash-dotted (red), and dash-dot-dotted (black) lines, respectively. Bottom: Normalized total spin angular momentum $\hat{L}^2/2N(2N+1)$ and von Neumann entropy of the ground state, denoted by solid (blue) and dash-dotted (red) lines, respectively. From left to right, we illustrate the corresponding expectation values and von Neumann entropy along four direct lines connecting four points—$O_{\rm AA}(-32,6)$, $O_{\rm CC}(32,6)$, $O_{\rm FF}(32,-6)$, and $O_{\rm PP}(-32,-6)$—in the parameter space of $(C_{12}\beta, C_{12}\gamma)/|C_1\beta_1|$. Intraspecies spin-exchange interactions are fixed at $(C_1\beta_1, C_2\beta_2)/|C_1\beta_1| = (-1,-2)$. The four lines are marked as dashed (red) lines in Fig. 1(a).

as a product state: $Z^{-1/2}(\hat{A}_0^{(2)\dagger})^{N/2}(\hat{B}_0^{(2)\dagger})^{N/2}|{\rm vac}\rangle$. We call the remaining phase the MM phase, which can show higher (lower) entanglement compared to the FF phase between the two species when $\beta > 0$ ($\beta < 0$). For the final case, when $\beta_1 < 0$, $\beta_2 > 0$, the ground state shows similar properties to that in the second case.

The most attractive phase when $\gamma = 0$ is the entangled ground state, denoted $\psi_{\rm AA}^{00}$ [19],

$$\psi_{\rm AA}^{00} = \frac{1}{\sqrt{2N+1}} \sum_{m=-N}^{N} (-)^{N-m} |N,m\rangle_1 \otimes |N,-m\rangle_2, \qquad (5)$$

which shows high entanglement with $S(\hat{\rho}_1) = 1$ between the two species. As demonstrated in Fig. 1 by numerical calculations, however, there remain other phases which show greater entanglement between the two species. This shows that state $\psi_{\rm AA}^{00}$ is not a maximally entangled state, in contrast to the previously studied case of two pseudo-spin-1/2 condensates [16]. This is not a surprise [28]. Due to the redundant degrees of freedom in the spin-1 case, the total spin angular momentum of each species can take values besides the largest value of N. To demonstrate the entanglement between the two species, we show their corresponding expectation values and von Neumann entropy along four lines connecting points $O_{\rm AA}(-32,6)$, $O_{\rm CC}(32,6)$, $O_{\rm FF}(32,-6)$, and $O_{\rm PP}(-32,-6)$ in the parameter space of $(C_{12}\gamma, C_{12}\beta)/|C_1\beta_1|$. The four lines are shown as the dashed (red) rectangle in Fig. 1(a).

In Fig. 3, we illustrate the ground-state properties of two ferromagnetic condensates with intraspecies spin-exchange interactions at $(C_1\beta_1, C_2\beta_2)/|C_1\beta_1| = (-1,-2)$. First, we consider the AA phase. When $\gamma = 0$, the spin-dependent Hamiltonian contains three operators commuting with each other, and the ground state can be expressed as $\psi_{\rm AA}^{00}$ for large enough antiferromagnetic interspecies spin-exchange interactions and shows high entanglement between the two species. When $\gamma \neq 0$, although the fourth term of the spin-dependent Hamiltonian does not commute with the other three, we find that the ground state not only shows similar expectation values of the operators, but also contains similar entanglement between the two species, over a large area in the phase diagram demonstrated in Fig. 1(a). For $\gamma < 0$, irrespective of its value, the ground state falls into the AA phase. For $\gamma > 0$, the ground state is still classified as the AA phase, as long as $C_{12}\gamma$ does not exceed a critical value, which increases in proportion to the interspecies spin-exchange interaction parameter $C_{12}\beta$. In the first column in Fig. 3, we evaluate the properties of the AA phase, where the ground-state expectation value of intra- and interspecies singlet-pairing number operators are close to 0, 0, and $N(N+2)$, respectively. The total spin angular momentum is exactly equal to 0, and the von Neumann entropy is close to 1.

When the interspecies singlet-pairing interaction exceeds a critical value, the ground state changes to the MM phase. As long as $C_{12}\gamma > 0$, it tries to decrease the interspecies singlet-pairing interaction. In the first column in Fig. 3, we follow the line of $O_{\rm AA}O_{\rm CC}$ and illustrate the phase transition from the AA phase to the MM phase. In the MM phase, as long as we increase $C_{12}\gamma$ accordingly, atoms in different species will continuously avoid pairing into singlets, while atoms in species 1 will try to pair into singlets. Atoms in species 2 first try to pair into singlets and then avoid pairing. Meanwhile, the total spin angular momentum first increases and then decreases. For a relatively large area of the MM phase, we find that the two species show high entanglement compared to the AA phase.

As the interspecies singlet-pairing interaction is increased, the ground state will fall into the CC1 phase, where its total spin angular momentum $\hat{L}^2$ will be equal to $N(N+1)$, and atoms in species 1 (2) will pair (not pair) into singlets. At the

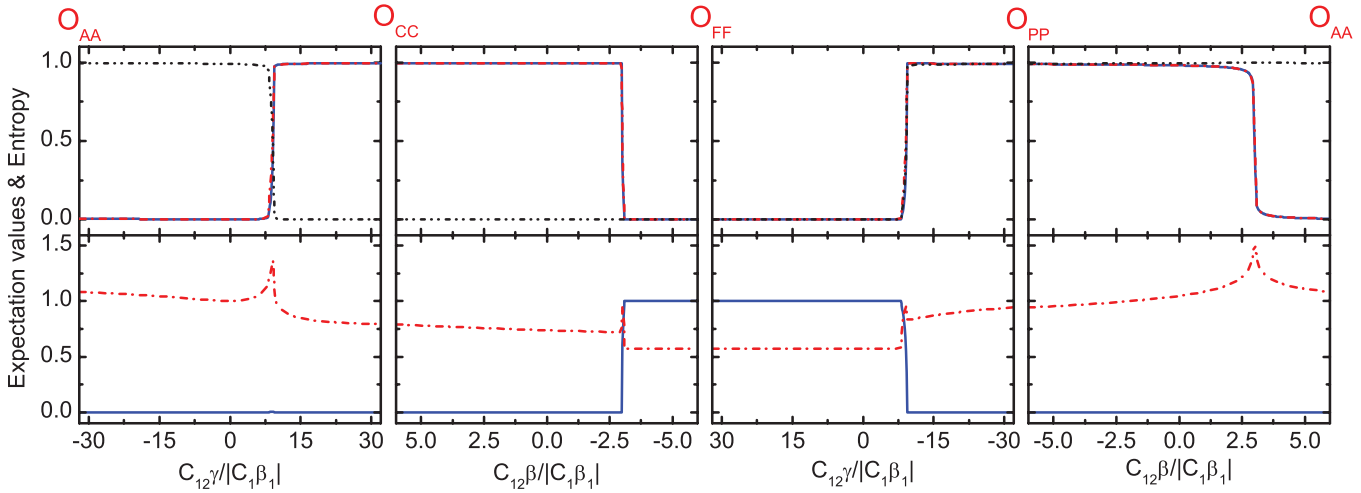

FIG. 4. (Color online) The same as that in Fig. 3, but with different intraspecies spin-exchange interactions fixed at $(C_1\beta_1, C_2\beta_2)/|C_1\beta_1| = (1,2)$.

same time, the expectation value of $\Gamma_0^{(1,1)\dagger}\Gamma_0^{(1,1)}$ will be near its maximum $N(N+2)$. The ground-state von Neumann entropy in the CC1 phase remains at a low value.

Going along the line $O_{\rm CC}O_{\rm FF}$, with decreasing interspecies spin-exchange interaction, the ground state changes from the CC1 phase to the MM phase and, finally, to the FF phase. Atoms of species 1 will become unpaired continuously, while the total spin angular momentum increases from $N(N+1)$ in the CC1 phase to its maximum $2N(2N+1)$ in the FF phase. The ground-state entanglement between the two species in the CC1 and the FF phase are almost at the same level. While in the MM phase, the entropy first increases to near 1 and then decreases.

We then follow the line $O_{\rm FF}O_{\rm PP}$. With decreasing interspecies singlet-pairing interaction, the ground state covers the FF, MM, and PP phases successively. In the PP phase, atoms in the same or in different species will all try to pair into singlets. The ground-state expectation values for intra- and interspecies singlet-pairing number operators will reach close to their corresponding maxima; meanwhile, the two species show higher entanglement. In the MM phase, the expectation values for operators or the von Neumann entropy change continuously to connect the FF phase and the PP phase.

Finally, we consider the line $O_{\rm PP}O_{\rm AA}$. As long as the interspecies spin-exchange interaction increases, the ground state will be changed continuously from the PP to the MM and to the AA phase. From the fourth column in Fig. 3, we find that over the whole line of $O_{\rm PP}O_{\rm AA}$, the two species show a relatively high entanglement, with the von Neumann entropy $S(\hat{\rho}_1)$ remaining higher than 1. This is especially so in the MM phase, where the highest entropy reaches 1.4568, which is close to the maximum entropy of $\log_{2N+1}[(N+1)(N+2)/2] \simeq 1.6116$.

In Figs. 4 and 5, we illustrate the two other cases, with intraspecies spin-exchange interactions $(C_1\beta_1, C_2\beta_2)/|C_1\beta_1|$ fixed at $(1,2)$ and $(-1,2)$, respectively. We find that the ground state shows similar properties to that in the two ferromagnetic condensates shown in Fig. 3. The only difference is for the CC2

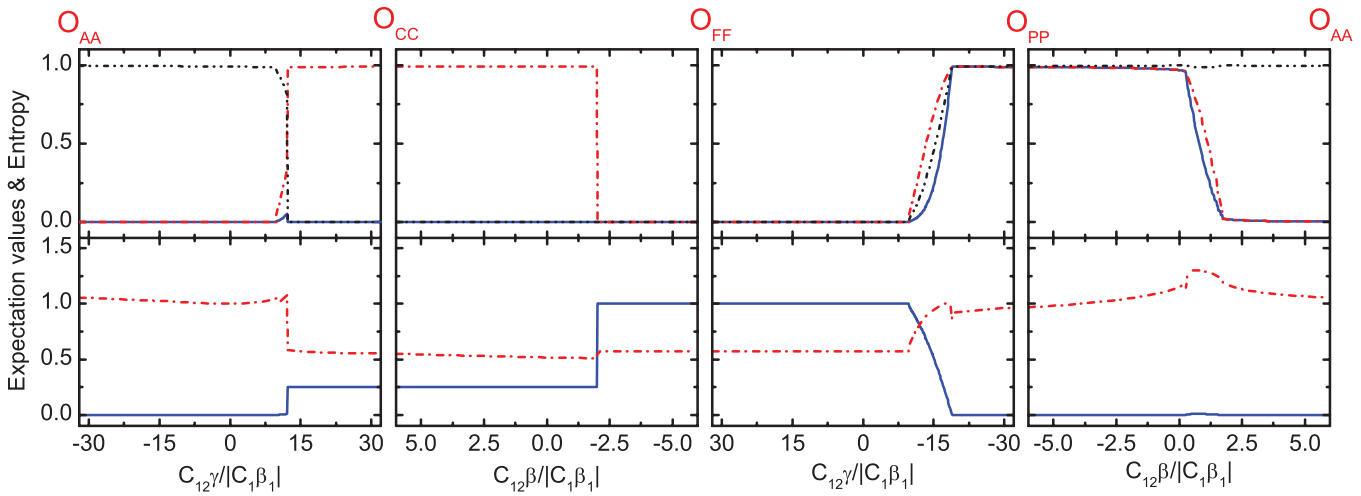

FIG. 5. (Color online) The same as that in Fig. 3, but with different intraspecies spin-exchange interactions, which are fixed at $(C_1\beta_1, C_2\beta_2)/|C_1\beta_1| = (-1,2)$.

or CC3 phase. In the CC2 phase, the ground-state expectation values for both intra- and interspecies singlet-pairing number operators are close to their corresponding maxima, $N(N+1)$, $N(N+1)$, and $N(N+2)$. While in the CC3 phase, they are close to 0, $N(N+1)$, and $N(N+2)$, respectively. The total spin angular momentum of the ground state is equal to 0 in the CC2 phase and to $N(N+1)$ in the CC3 phase. Meanwhile, in the CC2 phase the von Neumann entropy is less than 1 but higher than that in the FF phase, while in the CC3 phase, it is close to the value in the FF phase.

Before concluding, we wish to stress that the maximal entangled state in this system is given by

$$\psi_{\mathrm{ME}} = Z^{-1/2}\left(\hat{\Gamma}_0^{(1,1)\dagger}\right)^N|\mathrm{vac}\rangle. \tag{6}$$

It is the eigenstate or the ground state (if $\gamma < 0$) of the γ term in the Hamiltonian, Eq. (1), which means that the maximally entangled state ψ_{ME} is the eigenstate of two spin-1 condensates with only interspecies spin-singlet pairing interaction ($\beta_1 = \beta_2 = \beta = 0$ and $\gamma \neq 0$), with the corresponding eigenvalue $C_{12}\gamma N(N+2)/6$ [29].

V. CONCLUSION

In conclusion, we have studied the ground-state phase diagram for a binary mixture of two spin-1 condensates more carefully, going beyond the MF approximation. When no interspecies singlet-pairing interaction exists, the spin-dependent Hamiltonian contains three operators commuting with each other. In this special case, the most interesting phase is the AA phase, where two species show high entanglement. When interspecies singlet-pairing interaction is turned on, the added operators do not commute with the previous three operators, which forbids us from obtaining exact eigenstates analytically for the model spin system. In this study, we have performed full quantum diagonalization to find the ground states numerically. To quantify the ground states, we worked out the building blocks to construct the maximum spin states, which were used rightfully to discuss entanglement scales between the two species. We have evaluated the associated ground-state von Neumann entropy. After detailed calculations, we find that the AA phase can persist for large areas of the parameter space for interspecies spin-exchange and singlet-pairing interactions. In addition, there is another interesting phase, the PP phase, which shows a similar level of entanglement between the two species. What is more, we find that the AA phase is not the maximally entangled state. The ground state with the highest entanglement, we found, lies in the MM phase.

ACKNOWLEDGMENTS

This work was supported by the NSF of China under Grants No. 11004116, No. 10974112, and No. 91121005; the NKBRSF of China; and research program 2010THZO of Tsinghua University.

[1] S. Trotzky, P. Cheinet, S. Fölling, M. Feld, U. Schnorrberger, A. M. Rey, A. Polkovnikov, E. A. Demler, M. D. Lukin, and I. Bloch, Science **319**, 295 (2008); M. Lewenstein and A. Sanpera, Science **319**, 292 (2008).
[2] D. M. Weld and W. Ketterle, J. Phys. Conf. Ser. **264**, 012017 (2011).
[3] M. Ueda and Y. Kawaguchi, e-print arXiv:1001.2072.
[4] T.-L. Ho, Phys. Rev. Lett. **81**, 742 (1998).
[5] T. Ohmi and K. Machida, J. Phys. Soc. Jpn. **67**, 1822 (1998).
[6] C. K. Law, H. Pu, and N. P. Bigelow, Phys. Rev. Lett. **81**, 5257 (1998).
[7] M. Koashi and M. Ueda, Phys. Rev. Lett. **84**, 1066 (2000).
[8] C. V. Ciobanu, S.-K. Yip, and T.-L. Ho, Phys. Rev. A **61**, 033607 (2000).
[9] M. Ueda and M. Koashi, Phys. Rev. A **65**, 063602 (2002).
[10] S. Yi, Ö. E. Müstecaplıoğlu, C. P. Sun, and L. You, Phys. Rev. A **66**, 011601 (2002).
[11] T.-L. Ho and S. K. Yip, Phys. Rev. Lett. **84**, 4031 (2000).
[12] T.-L. Ho and L. Yin, Phys. Rev. Lett. **84**, 2302 (2000).
[13] E. J. Mueller, T.-L. Ho, M. Ueda, and G. Baym, Phys. Rev. A **74**, 033612 (2006).
[14] A. B. Kuklov and B. V. Svistunov, Phys. Rev. Lett. **89**, 170403 (2002).
[15] S. Ashhab and A. J. Leggett, Phys. Rev. A **68**, 063612 (2003).
[16] Y. Shi and Q. Niu, Phys. Rev. Lett. **96**, 140401 (2006).
[17] M. Luo, Z. Li, and C. Bao, Phys. Rev. A **75**, 043609 (2007).
[18] Z. F. Xu, Y. Zhang, and L. You, Phys. Rev. A **79**, 023613 (2009).
[19] Z. F. Xu, J. Zhang, Y. Zhang, and L. You, Phys. Rev. A **81**, 033603 (2010).
[20] J. Zhang, Z. F. Xu, L. You, and Y. Zhang, Phys. Rev. A **82**, 013625 (2010).
[21] Y. Shi, Phys. Rev. A **82**, 023603 (2010).
[22] Z. F. Xu, J. W. Mei, R. Lü, and L. You, Phys. Rev. A **82**, 053626 (2010).
[23] Y. Shi and L. Ge, Phys. Rev. A **83**, 013616 (2011).
[24] J. Zhang, T. Li, and Y. Zhang, Phys. Rev. A **83**, 023614 (2011).
[25] M. W. Jack and M. Yamashita, Phys. Rev. A **71**, 033619 (2005).
[26] Y. Wu, Phys. Rev. A **54**, 4534 (1996).
[27] The total Hilbert space for zero magnetization, $l_z = 0$, for the case where $N_1 = N_2 = 100$ is 174 301. Here we use the ARPACK package to do numerical diagonalization.
[28] Ö. E. Müstecaplıoğlu, M. Zhang, and L. You, Phys. Rev. A **66**, 033611 (2002).
[29] We previously miscalculated the operator $\hat{\mathcal{S}}_z$, which is equal to $(\hat{N}_1 + \hat{N}_2 + 3)/2$, not $(\hat{N}_1 + \hat{N}_2)/2 + 3$ as stated in Ref. [19]. As a result, $\mathcal{S} = (n_0 + 3)/2$ ($n_0 = 0,1,2,\ldots$), $\min(\mathcal{S}) = 3/2$, and $\min(\mathcal{S}_z) = 3/2$. Also, Eq. (13) in Ref. [19] needs to be changed to $E = \frac{1}{4}C_{12}\beta l(l+1) + \frac{1}{6}C_{12}\gamma n_s(n_s + n_0 + 2) - \frac{1}{2}C_{12}\beta(N^{(1)} + N^{(2)})$.